NOVEL MONO-CRYSTALLINE SOLAR CELLS WITH IMPROVED EFFICIENCY

Alex Axelevitch and Gady Golan

Holon Institute of Technology – HIT, Holon (Israel)

1. Introduction

Solar cells, as alternative energy sources, attract much attention in recent decades. Solar cells have the potential to replace fossil fuels as the main means of electric power generation. However, solar cells of all types suffer of two main deficiencies: relatively low efficiency, and high cost in comparison with conventional fossil fuel electric sources. It's known that the maximum theoretical efficiency of solar light to electricity conversion, may reach to approximately 93%. Also it's known that obtained solar power in earth is about 1.2×10^{17} W. Thus, there are significant reasons to put efforts and resources to develop low cost and high efficient PV convertors.

The chart presented in figure 1 shows the best laboratory photovoltaic efficiencies obtained for various materials and technologies [1]. Usually, this is done for very small, 1 cm^2, solar cells and requires application of concentrators, cooling systems, and complicated technologies such as multi-layer thin film semiconductor systems. These systems must take into account a variety of technological and material parameters such as: semiconductor lattice parameters, formation temperatures and working temperatures, refraction coefficients matching, thickness of all layers in the multi-layer system, concentration of charge carriers in the semiconductor layer, and many others.

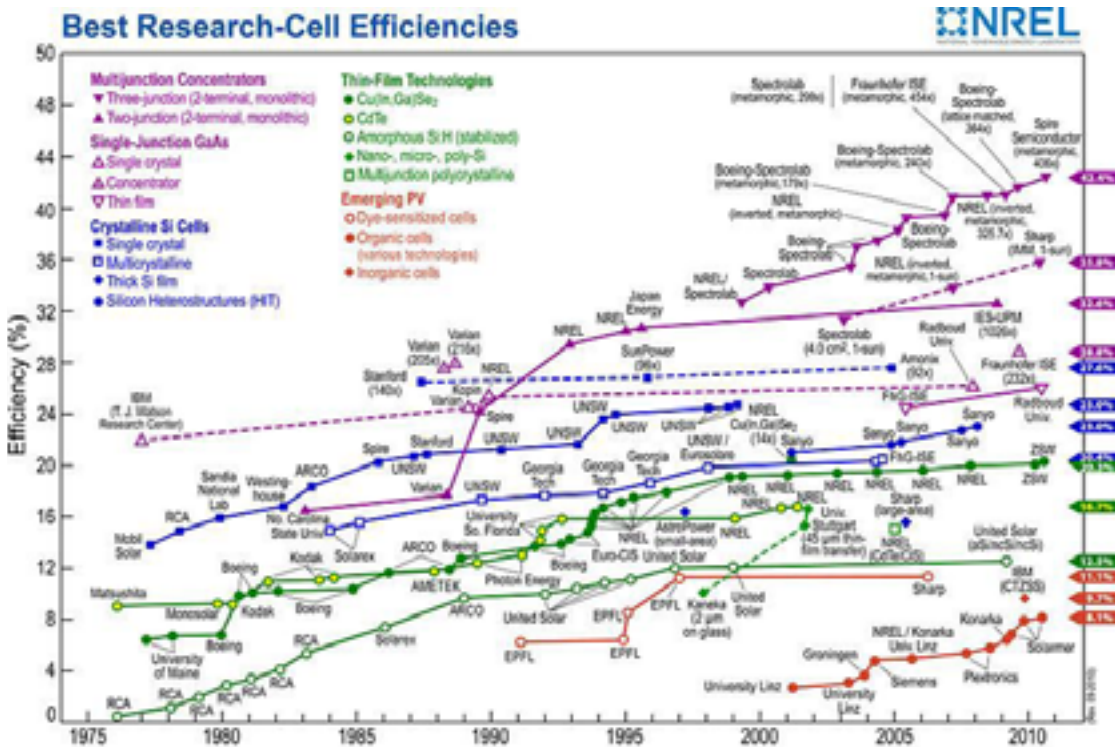

Fig. 1: NREL compilation of best research solar cell efficiencies [1]

Almost 90% of all solar cells produced in 2006 were made from single and polycrystalline silicon. Significant growth of silicon consumption in the world results in an increase in silicon price due to the solar cells market appearance together with the microelectronics industry. Single crystalline silicon solar cells are the most widely used today. Together with the polycrystalline cells which are slightly less efficient, they represent the base line of the nowadays market. At the same time, thin film solar cells made of amorphous silicon (a-Si) became significant in the commercial photovoltaic device market. Amorphous silicon solar

cells can be made in many combinations using a wide variety of substrate materials, including flexible ones. Unfortunately, solar cells made by chemical vapor deposition (CVD) methods suffer of low efficiency and significant degradation under solar irradiation (the Staebler-Wronski effect). Also, due to the small thickness of the semiconductor layers, a substantial part of the solar light cannot be absorbed (photons with wavelength of more than 800 nm).

Unfortunately, the extremely high conversion efficiency is not feasible in practical devices due to losses caused by electrical, optical, material and technological reasons. Optical losses reduce the level of solar radiation by reflection and shadowing of the irradiating light. The spectral sensitivity of various semiconductors has a significant contribution to the optical losses. All photons with energy lower than the semiconductor band-gap cannot generate electron-hole pairs and thus lost in the semiconductor substrate. Photons with energy that is higher than the bandgap generate charged carriers which transfer additional energy to the semiconductor material (the thermalization process) and heat up the photovoltaic device. This increasing heat decreases the cell's efficiency. Electrode system (pass-bars), located on the active surface of the solar cell, also reduces the efficiency by reducing the surface area that absorbs light.

Electrical losses have detrimental effects on both the current and the voltage of a solar cell. These losses may be conditionally divided to two major groups: losses due to the electrical transport (Ohmic losses) and recombination losses given by various recombination mechanisms. The Ohmic losses consist of electrical resistance to transport of charged carriers within the doped regions of the device: emitter and base, resistance of the P-N junction, contact resistances on the borders of the semiconductor and metal collectors, and the resistance of thin metal films of the collector system. The recombination losses are defined by various processes in the semiconductor: a radiative or "band-to-band" recombination (luminescence), Auger recombination, recombination on the semiconductor defects and impurities (Shockley-Read-Hall or SRH recombination), and surface recombination. Detailed analysis of electrical losses was done in past by many authors [3, 4].

Losses due to the properties of the used materials and the characteristics of the applied technologies also seriously affect the efficiency of converting light into electricity. These losses are determined by a plurality of different independent factors, incorrect selection of which can lead to complete failure of solar cells. Consequently, the appropriate technology must take into account all possible mechanisms of losses and reduce the influence of each of them.

As mentioned above, an intrinsic layer of semiconductor may be inserted between the doped parts of a diode-type PV cell, to increase the active converting region. The following parts of this paper present an analysis of the influence of the intrinsic layer on the efficiency of solar cells, a new design of solar cell, developed on the basis of this analysis, and a new technology to manufacturing novel highly efficient solar cells.

2. Efficiency of the PIN system

2.1. PN structure performance

Figure 2 presents schematic cross-section of the non-ideal conventional diode-type PV cell. Photon with suitable energy may be absorbed by the semiconductor material. This process consists of generation of charged carrier pair: electron and hole. Due to the built-in electrical field within the P-N junction, these charged carriers are drifted to the emitter (electrons) and to the base (holes) thus generating electric current which is applied to the external load. Figure 2c represents the simplest case of electrical charge distribution. Assuming an abrupt type of the junction, the cross-section (Fig. 2a) represents three actual regions in the PV cell: emitter (an n-type layer), base (p-type layer), and the space-charge region (depletion zone of the formed junction).

We assume that light irradiation penetrates the cell as a flux of photons (as shown in figure 2b) and that the cell (crystalline structure) absorbs the light homogeneously, in the first approximation. The quantity of the excess charged generated pairs, $\Delta n = \Delta p$ is lower than the majority carrier concentration. Only the minority charged carriers generated in both sides of the diode under irradiation can be taken into account for the

charge collection. Thus, only electrons generated in the p-type base, in a distance of electron's diffusion length from the depletion region, may reach the electron collector. The same part of holes generated in the emitter can reach the hole collector. However, charged carriers of both types generated in the depletion zone are effective due to $\Delta n > n_i$, the intrinsic concentration of the charged carriers.

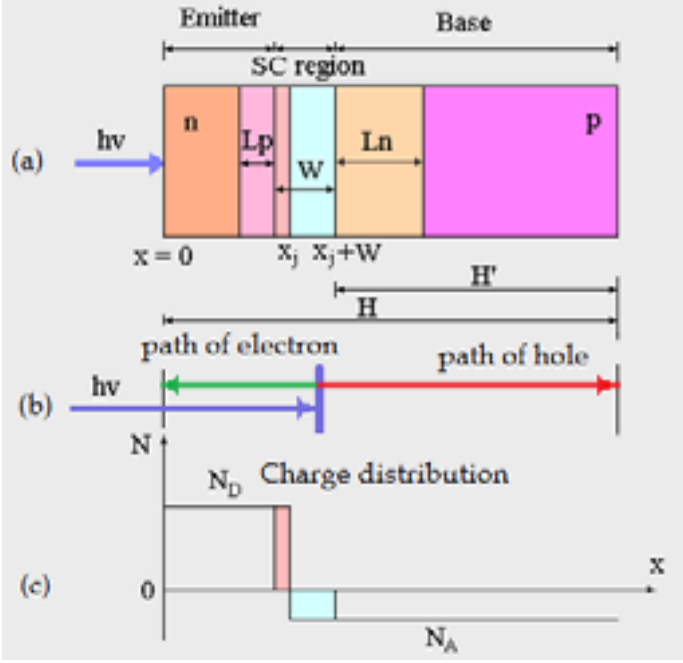

Fig. 2: Cross-section of the non-ideal diode-type PV

All of the current processes in the PV cell may be described by Poisson's equation and the continuity equation. Detailed analysis of these processes shows that the current density generated by diode-type solar cell is described by follows equation:

$$J = J_p + J_n + J_R = J_0\left(e^{\frac{V}{V_t}} - 1\right) - qG\left(L_p + L_n + W\right) \quad \text{(eq.1)}$$

Where J_p, J_n, and J_R are current density generated in the base, emitter and space charge region respectively, L_p and L_n are holes and electron diffusion length respectively, $V_t = kT/q$ is the environment potential, k is the Boltzmann's constant, T is the absolute temperature of the environment in K, V is the voltage generated by the cell due to the charges separation, W is the space charge region width as shown in figure 2a, q is the electron's charge, G is the electron-hole pairs generation rate, and J_0 is the leakage current density, described by follows relation:

$$J_0 = qn_i^2\left[\frac{D_p}{L_p N_D} + \frac{D_n}{L_n N_A}\right] \quad \text{(eq.2)}$$

Where N_D and N_A are the impurity concentrations in the emitter and base respectively, D_p and D_n are hole's and electron's diffusivity respectively, and n_i is the intrinsic charge carriers concentration.

To compare values of W, L_n and L_p for conventional silicon diode, we have calculated these values, as they are fully defined, by the silicon properties and the impurity level concentration in the p- and n-sides of the structure. Table 1 present the silicon properties required for calculation at room temperature [4].

Tab. 1: Properties of the silicon

Property	Units	Value
Intrinsic carriers concentration	cm^{-3}	1.5×10^{10}
Relative dielectric constant, ε_r	-	11.7
Electron mobility, μ_n	$cm^2/v\times s$	1350

Holes mobility, μ_p	$cm^2/v\times s$	480

The calculation was performed for two different diode structures with different impurities concentration and for the condition of equal lifetime of generated charged carriers ($\tau_n = \tau_p = 0.1\mu s$), see the table 2. Also, an electrical field providing separation of the generated charged carriers was calculated. For these calculations we will use the well known following relations:

The built in potential: $V_b = V_t \ln\frac{N_A N_D}{{n_i}^2}$ (eq.3)

The depletion zone width: $W = \sqrt{\frac{2\varepsilon_0\varepsilon_r V_b}{q}\left(\frac{1}{N_A}+\frac{1}{N_D}\right)}$ (eq.4)

The diffusion length: $L = \sqrt{D\tau}$, where $D = \mu V_t$ (eq.5)

The maximum electrical field: $E_m = -\frac{qN_A x_p}{\varepsilon_0\varepsilon_r} = -\frac{qN_D x_n}{\varepsilon_0\varepsilon_r}$ (eq.6)

Here, x_p and x_n are the depletion width in the p-side and n-side of the junction, respectively.

Tab. 2: Calculation results of the width for two different diode structures.

N	N_A	N_D	V_b	W	L_n	L_p	$-E_m$
	cm^{-3}	cm^{-3}	V	μm	μm	μm	$\times10^4$ V/cm
1	10^{16}	10^{16}	0.7	0.43	18.7	11.1	3.2
2	10^{16}	10^{19}	0.88	0.34	18.7	11.1	5.3

In the table, V_b represents the built-in potential of the diode and E_m is the electrical field value. As shown, the space charge region takes a small part of the effective zone. However, we can significantly increase the generated current by widening the space charge region (see equation 1). This may be performed by introducing additional intrinsic (i-) semiconductor layer between the p and n parts of the diode system. So, we will obtain the PIN structure instead of PN.

2.2. PIN structure performance

The main difference between the PN-diode and the PIN diode is the extension of the internal electric field in the diode [5]. The internal electric field is limited to the depletion layer in the PN-type diode, whereas it extends over the whole i-layer in the PIN-type diode. The operating principle of photovoltaic solar cell is generation of charged carriers under irradiation and their separation by the internal built-in electric field. So, location of this electric field and its value are most significant. The internal electric field must provide a complete separation to the generated charged carriers and its maximal utilization. Generally, the distance of traveling from the origin point to the suitable electrode is determined by the carrier diffusion length. Maximum value of this parameter may reach the order of 1 cm for the single-crystalline Si or Ge [6]. In the case of a PIN-diode structure, collection of the charged carriers is governed by the drift length of both electrons and holes within the intrinsic layer. It can be shown, that, under "reasonable conditions", the drift value is about 10 times larger than the minority carrier diffusion length [7]. Thus, if the quality of the applied material is high, the high efficient PIN solar cells based on the single-crystalline silicon may be achieved. This claim was verified using the "Afors-Het" simulation program [8].

We considered a virtual photovoltaic structure, presented in figure 3. This structure represents a single-crystalline p-type silicon substrate, 2 mm thick, equipped at its rear side by continuous metal electrodes. The front side of the substrate is coated respectively by an intrinsic silicon layer of 1 μm thick, a 2 μm thick single-crystalline n-type silicon layer, and a 150 nm thick layer made of indium-tin oxide (ITO) film. This upper layer is coated with a pass-bar electrode net representing the upper electrode.

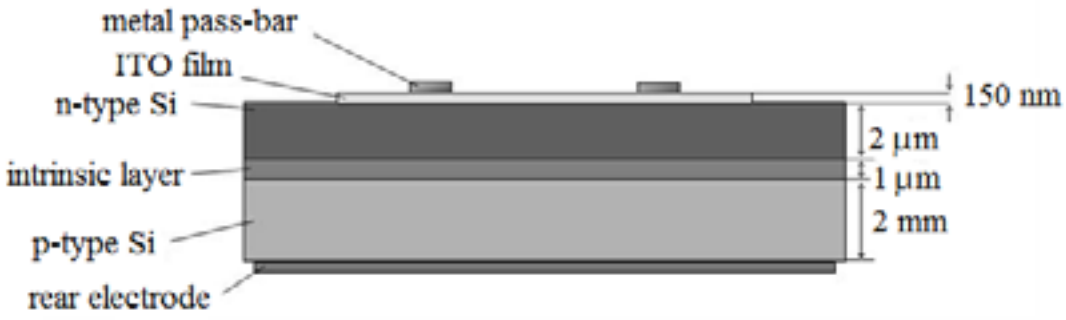

Fig. 3: Virtual PV structure for evaluation of the intrinsic layer influence

The I-V characteristics, simulated by the "Afors-Het" program, for the PV structure presented in figure 3, are shown in figure 4 for the standard conditions of room temperature and irradiation of AM1.5 solar spectrum with an average power of 1000 W/m^2.

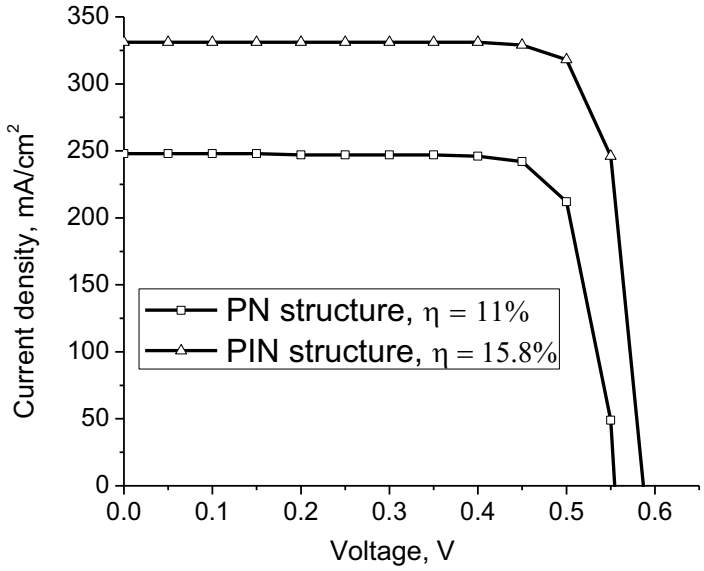

Fig. 4: I-V characteristics for PN and PIN structures simulated by "Afors-Het"

Estimated difference in the efficiency shows an increase of the PIN structure in almost 5% for the considered non-optimized virtual structure. This system is better than the conventional PN structure; however, it suffers from the following disadvantages:

- There are difficulties in growing single crystalline silicon layers as intrinsic as highly doped;
- Efficiency of the PIN structure decreases due to the existence of the upper pass-bars which shade a significant part of the active front surface of the PV cell;
- The large thickness of the base layer decreases the number of excess holes that can reach the rear electrode;
- The separated by the internal electric field charged carriers must overcome the highly doped emitter layer. This layer increases their electrical loss due to Auger recombination;
- As emitter as base - both increase electrical losses due to Shockley-Read-Hall (SRH) recombination processes;
- The active part of the structure is comparatively thin, thus decreasing the number of excess charged pairs, generated by light irradiation.

It seems that high efficiency solar cell should be free from the above mentioned shortcomings.

3. Novel construction of the solar cell

It can be seen in figures 2 and 3 that photons penetrating through the front surface of the cells generate electrons and holes which move in the same direction of photons (holes) and in opposite direction (electrons). This conventional system is designated as a "vertical behaving system". Photons coming from the top and charged carriers move in parallel or anti-parallel to photons. Let's turn this construction so that charged particles begin to move now perpendicular to the direction of the incoming photons. Let's also widen the intrinsic zone and make emitter and base significantly thinner. A cross-section of such novel PIN construction of the PV cell is presented in figure 5. This PV cell represents a single-crystalline silicon strip, ~ 10 mm wide and 10 cm long, having the maximal surface area of 10 cm^2 oriented accordingly [001] direction. This silicon is grown as pure single crystal material having intrinsic concentration of charged carriers ($n_i \approx 1.5\times10^{10}$ cm^{-3}). Both sides of the strip are heavily doped by donors at one side ($N_D \approx 10^{19}$ cm^{-3}) and by acceptors on the other side ($N_A \approx 10^{19}$ cm^{-3}). Both sides are also coated by metal electrodes with Ohmic contacts.

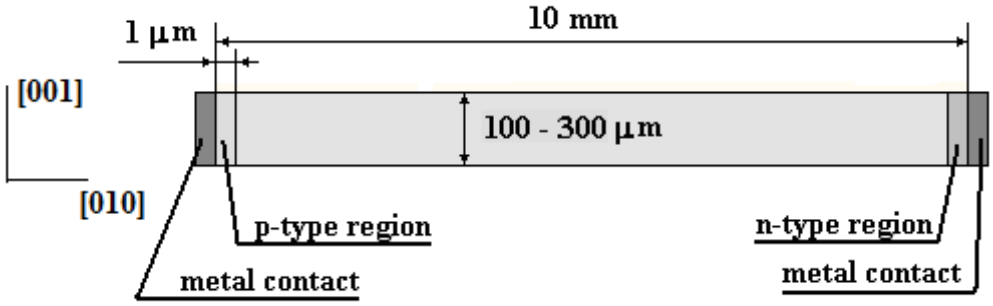

Fig. 5: Novel PIN construction of the PV cell

Figure 6 represents approximately a charge distribution in the novel cell (fig. 6 c), an internal electrical field distribution (fig. 6 d), and directions of incoming photons and generated charged carriers (fig. 6 a). This structure may be designated as "lateral PV cell" due to the perpendicular direction of charged carriers moving relative to the photons incoming.

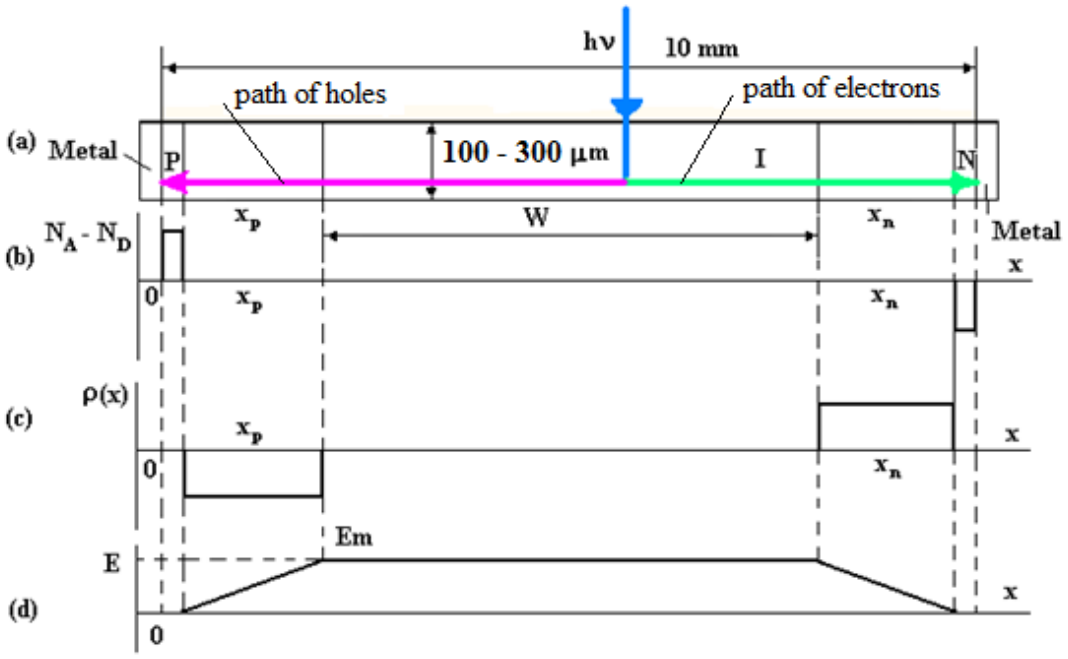

Fig. 6: A cross-section view of the novel solar element

What can we see in this construction: first of all, an active surface which absorbs the photons occupies almost the entire surface of the PV cell. This wide active intrinsic zone is totally un-doped. Consequently, the SRH recombination caused by impurities is practically absent. The obtained silicon strip is oriented according to the [100], [010], [001] directions, hence most of the charged carriers move now via virtual free

channels. Thus, the carriers are practically free of collisions with lattice atoms and are scattered only by crystal defects. As a result of that the mean free path of the charged carriers and their mobility reaches its maximum value. Since the main mechanism of separation of the generated charged carriers is the internal built-in electric field, it is interesting to calculate its value and its spatial distribution to achieving complete charge separation in this novel system.

To find the correct description of the PIN structure behavior, we have to consider physical processes at p+/i (or n+/i) junctions in detail. The full-depletion approximation assumes that the depletion region around the metallurgical junctions has well-defined edges [9]. It also assumes that the transition between the depletion region and the quasi-neutral region is abrupt. Here, the quasi-neutral region is defined as the region adjacent to the depletion region. In the quasi-neutral region, the electric field is small and the free carrier density is close to net doping density. The PV cell shown in figure 6 has the abruptly doped sides that may be realized enough simple, for example by an epitaxial growth process. Also, the quasi-neutral region is not doped, thus it contains the inrinsic charged carriers only. However, we cannot claim that the depletion regions closed to the quasi-neutral sides are free of the mobile charged carriers due to dynamical type of equilibrium processes in the junctions. Therefore, for the description of this device we must use the Poisson's equation without the depletion approximation part. In other words, we must admit that mobile charged particles are exists and move within the depletion zone.

The one-dimensional general form of the Poisson's equation for the potential distribution looks as follows:

$$\frac{d^2\emptyset}{dx^2} = -\frac{\rho}{\varepsilon_s} = -\frac{q}{\varepsilon_s}(p - n + N_D - N_A) \quad \text{(eq.7)}$$

Here, $\varepsilon_s = \varepsilon_0\varepsilon_r$ is a relative dielectric constant and the charge density, ρ, is taken as a function of the electron density, the hole density and the impurities density. To solve the Poisson's equation, the electron and hole's density may be written as functions of the potential ϕ using the Fermi level, ϕ_F, defined for an intrinsic semiconductor as follows:

$$\emptyset_{Fi} = \frac{E_g}{2} + \frac{3}{4}kTln\left(\frac{m_h^*}{m_e^*}\right) \quad \text{(eq.8)}$$

Where E_g is the bandgap of our semiconductor and m_e^* and m_h^* are effective mass of electron and hole respectively. For the doped semiconductor (for example, p-type) this relation takes following form:

$$\emptyset_F = \emptyset_{Fi} - kTln\left(\frac{N_A}{n_i}\right) \quad \text{(eq.9)}$$

Therefore, the Poisson's equation may be rewritten as follows:

$$\frac{d^2\emptyset}{dx^2} = \frac{2qn_i}{\varepsilon_s}\left(sinh\frac{\emptyset-\emptyset_F}{kT} + sinh\frac{\emptyset_F}{kT}\right) \quad \text{(eq.10)}$$

Where $sinh\frac{\emptyset_F}{kT} = \frac{N_A-N_D}{2n_i}$ (eq.11)

We have obtained the second-order non-linear differential equation which cannot be solved analytically in the general case. However, it can be simulated using suitable simulation software in each specific case.

4. Simulation

Simulation of our novel PV cell had to meet the following questions:

1. How wills the built-in electrical field in the lateral PIN structure is distributed?
2. Which mechanism drives the charged carriers in this structure?
3. What efficiency may be reached in this lateral PIN structure?
4. By-facial mode of operation – possibility for application.

5. Evaluation and influence of factors such as width of the I-region, level of irradiation, level of doping in cathode and anode, temperature of the basic PV cells (open circuit voltage, short circuit current, efficiency).

In order to check the distribution of the built-in electrical field at the junction between the side electrode (anode or cathode) and in the intrinsic region, a numerical simulation was peformed. We assumed an abrupt PIN diode structure with variable width W and the thickness D = 300 μm under equilibrium in dark condition. The side electrode's doping concentration was chosen as $N_D = N_A = 10^{20}$ cm^{-3}.

This simulation was done using the Silvaco's ATLAS silicon device simulator based on the "Synopsys". The concentration value in the intrinsic zone was chosen at the ν-level ($N_D \approx 10^{12}$ cm^{-3}). The simulation shows that the field strength reaches high values of tens of thousands Volts per centimeter for sufficiently small size of the intrinsic zone (up to 2 microns) in defined conditions. In 10 microns within the intrinsic zone, the field drops to hundreds of Volts per centimeter and after 50 microns the field practically disappears. Figure 7 presents the electrical field distribution for the equilibrium state and without irradiation.

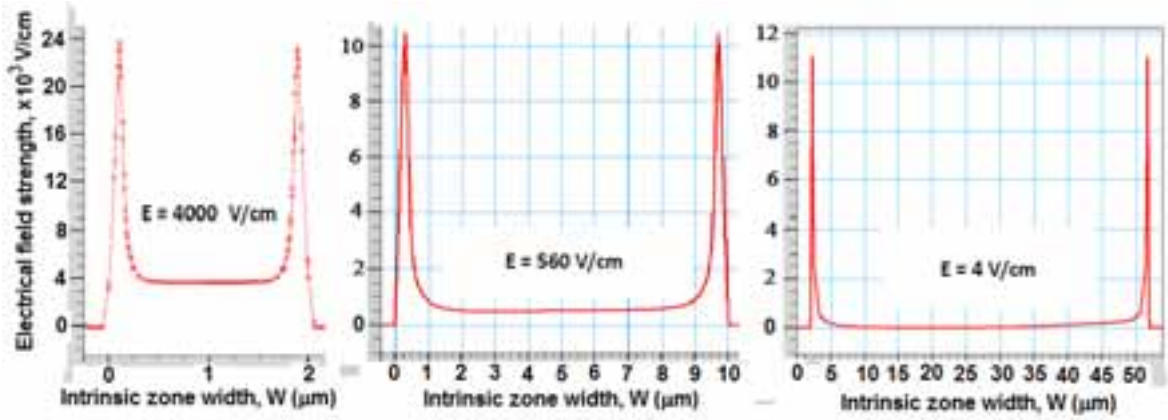

Fig. 7: Electrical field strength for various intrinsic zone widths

As shown in Fig. 7, the electrical field drops practically to zero at dark equilibrium conditions. However, the irradiation drastically changes this picture. The following simulation was provided for a sample having a doping concentration in both sides, equal to 10^{19} cm^{-3} and wide width relative to the sample presented in figure 7, W = 1 mm. In this experiment, the passivated sample was illuminated by monochromatic light with a wavelength of 800 nm in various intensities from one side. The passivation layer thickness was of 70 nm. The MINIMOS-NT device simulator developed for simulation of MIS solar cells [10] was used. Fig. 8 presents the simulation results.

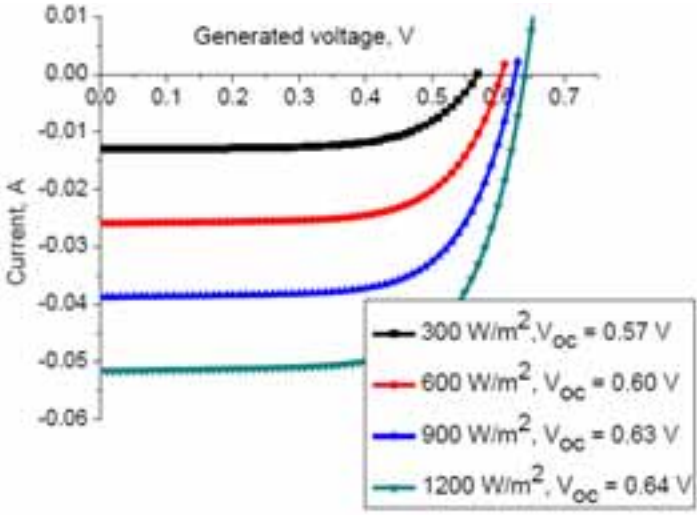

Fig. 8: I-V characteristics for various light intensities

Here, no contact resistance was taken. However, SRH and surface recombination are accounted for. As shown in Fig. 8, our novel PV cell construction generates electricity according to the received light energy. Also, as shown in Fig. 5, this construction of PV cell enables bi-facial illumination. Simulation of bi-facial illumination shows a double growth of electricity generated. In order to clarify what mechanism is responsible for the charge separation in the cell, the simulation of electrical fields in both cases: dark and illumination, was done. Fig. 9 compares the electric field in 1 mm width cell with and without irradiation at zero bias.

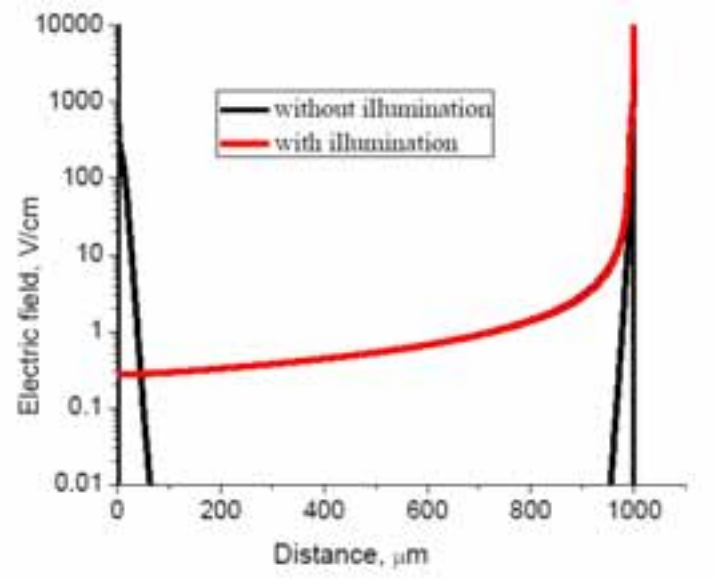

Fig. 9: Electric field along the cell width

As shown, the electric field looks different in the two simulated cases. In case of darkness, there is a high electric field near the contact. This field drops very quickly with the distance. A slope of the doping profile, defined in a distance of 1 μm, leads to a reduction of the peak electric field from 30 kV/cm to almost zero. This picture dramatically changes with illumination. Now, the field is able to separate the charges and transfer them to the electrodes. In this case, the dominant transport mechanism is a drift in the electric field.

Fig. 10 presents a by-facial simulation of the cell behavior with different trap concentration. The trap concentration value $N_t = 10^{12}$ cm^{-3} is very high for intrinsic silicon. If we decrease the trap concentration to value $N_t = 10^{10}$ cm^{-3} or simulate the cell behavior without SRH recombination, we obtain a significant increase of I_{sc} (short-circuit current) and V_{oc} (open circuit voltage).

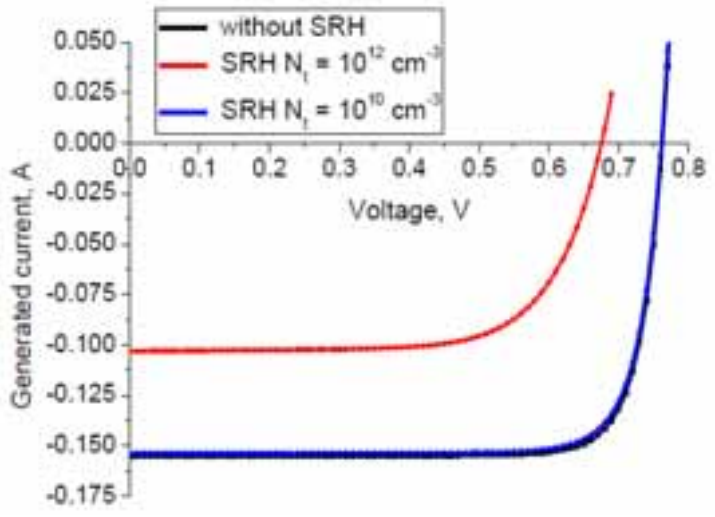

Fig. 10: I-V characteristics for various SRH recombination

As shown in Fig. 10, a number of traps (crystal defects, impurities etc.) in silicon strongly affect its transport properties. Therefore, the silicon must be pure, single crystalline and properly positioned for PV cells preparation. The crystal should be oriented in the [100], [010], and [001] directions to minimize the transport collisions and increase the carriers lifetime. For example, lifetime of 10 ms was obtained for charge carriers in the case of $N_t = 10^{10}$ cm^{-3}.

The novel PV cell behavior significantly depends on the ambient temperature. This PV cell is made of pure single-crystalline silicon with intrinsic concentration of charged carriers. Their concentration is proportional to the temperature in degrees γ ($\gamma \approx 1 \div 4$) that leads to dependence of V_{oc} from temperature. This dependence may be described as follows [3]:

$$\frac{dV_{oc}}{dT} = -\frac{V_g - V_{oc} + \gamma V_t}{T} \quad \text{(eq.12)}$$

For silicon the estimation according to eq.12 gives a reduction in the open circuit voltage of about 2.3 mV per ^{0}C. Fig. 11 presents our simulation results of our novel PV cells with various ambient temperatures T = 300-400 K. As shown in Fig. 11, while a short circuit current I_{sc} remains nearly the same, V_{oc} decreases with reduction of ~2 mV/K.

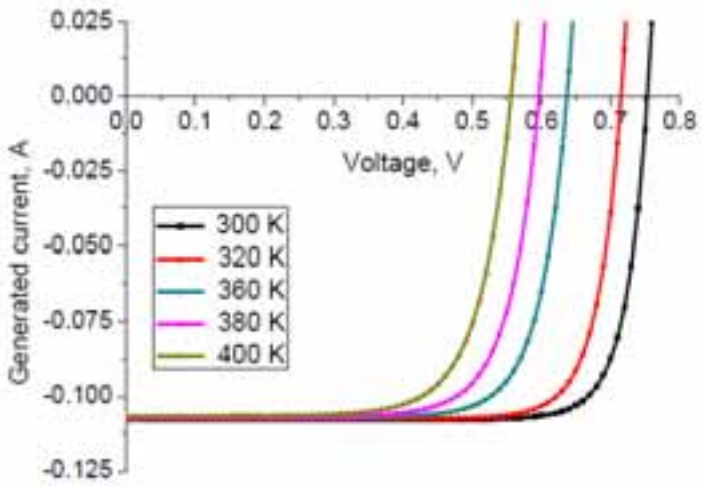

Fig. 11: I-V characteristics for different temperatures

All of the above simulations were done for cell's width of W = 1 mm. However, the real cell's width should be higher. Fig. 12 presents simulations for the cells with various widths from 1 mm to 20 mm.

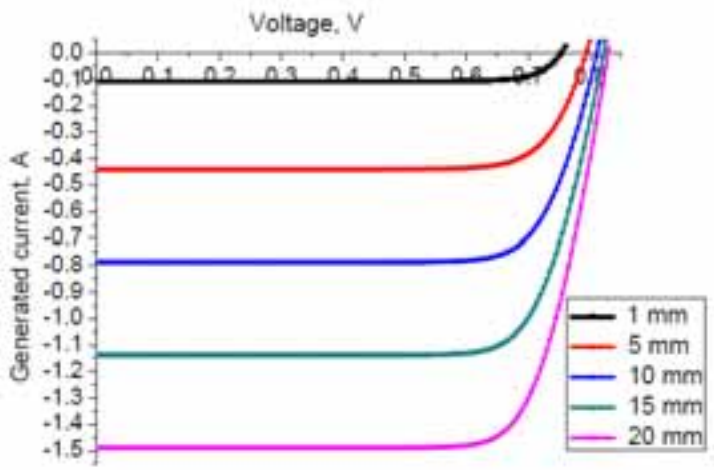

Fig. 12: I-V characteristics for various cell widths

These simulations were based on illumination according to the ASTM G173-03 reference spectra, which gives after integration 832 W/m^2 power intensity for the range: λ = 400-1000 nm and for integral solar power intensity of 1200 w/m^2. Simulations were performed without recombination and without reflections. As

shown, the generated electricity grows proportionally to the received solar power. Evidently, electricity losses also grow together with the width growth. Fig. 13 presents the maximum generated power (P_{max}, W), fill factor (FF, %), and efficiency (η, %) as functions of the cell's width.

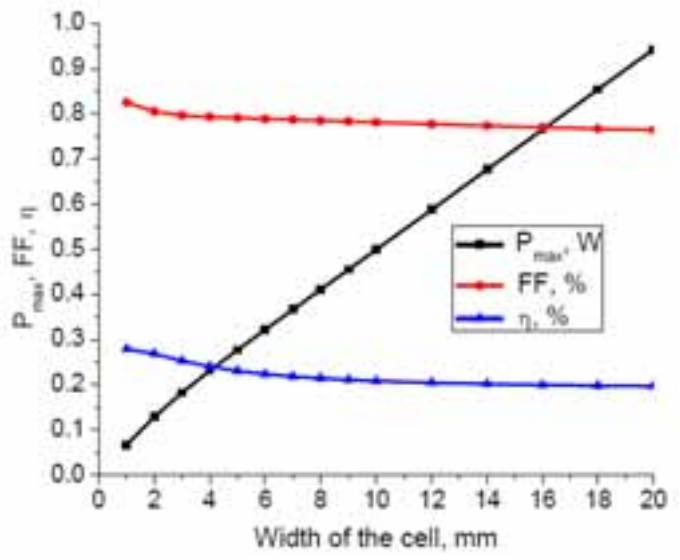

Fig. 13: Maximum power, fill factor, and efficiency vs. cell width

As can be seen from the graphs, the maximum efficiency reaches 28% for narrow cells and slightly reduced for wider cells. The results of these simulations give hope for high efficiencies results to our novel PV cells in their lateral mode of operation.

5. Experimental Implementation

Practical implementation of our novel PV cell was based on a patent application of Golan et al, (2011). There are some problems in carrying out experimental verification of novel type of PV cells. Almost all global manufactured single-crystalline silicon is P type. This is due to the requirements of the microelectronics industry which is a major player in the silicon market. Thus, the silicon which is used in our experiments was P-type with resistivity of about 10 kΩ×cm. This resistivity corresponds to impurities concentration of about $N_t = 1.4\times10^{12}$ cm^{-3}. Such number of traps leads to SRH recombination and consequently to an increase in the cell's losses.

The second challenge was to create highly doped (~10^{19} cm^{-3}) regions with abrupt transition at the edges of the cell. Such technologies are not developed yet and are subjected to scientific and technical development. Same can be said on making Ohmic contacts into the doped regions. In our case, the highly doped regions at the edges of the samples were made by diffusion of boron and phosphorus, respectively. Contacts to the doped sides of the samples were done using metal-brazing pastes. Passivation of the samples was done using plasma enhanced chemical vapor deposition (PECVD) reaction. The oxy-nitride films with thickness of approximately 70 nm were grown on the silicon samples on one side. These films also play the role of antireflection coatings. Measured lifetime of the charged carriers under the passivation layers was of 5-10 ms. The measured minority carriers diffusion-length was of ~4 mm. The schematic view of the complete PV cell is presented in Fig. 14.

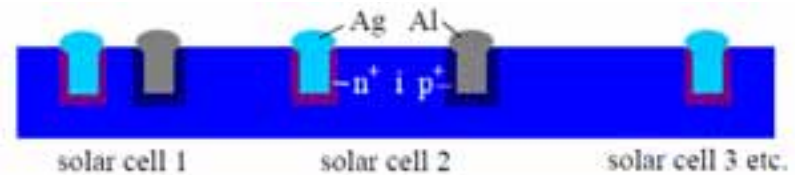

Fig. 14: The schematic view of the novel PV cell

Efficiency of the first examined PV cells has reached η = 11.9 % and FF = 79.6 % for one-side illumination.

6. Conclusions

Based on the simulation experiments and first trials of practical implementation of our novel type of PV cells, we can conclude the following:

1. The lateral structure is preferred on the vertical;
2. Despite the large width of cells, the electric field generated in the semiconductor under illumination is sufficient for efficient charged carriers separation;
3. The lateral construction provides full utilization of the active PV cell surfaces;
4. The lateral construction and right choice and orientation of the semiconductor crystal enables us to minimize losses due to SRH and surface recombination mechanisms;
5. These PV cells can be used in a bi-facial illumination mode;
6. The maximal efficiency of these PV cells under bi-facial illumination can reach 28%;
7. This lateral structure of PV cell can be easily implemented into a manufacturing process.

7. References

1. Lawrence Kazmerski, "NREL compilation of best research solar cell efficiencies", National Renewable Energy Laboratory (NREL), 2010, http://en.wikipedia.org/wiki/File:PVeff(rev100921).jpg
2. Goetzberger, A., J. Knobloch B., 1998. Voβ, Crystalline Silicon Solar Cells, John Wiley & Sons, Chichester.
3. Axelevitch A., Golan G., 2010. Efficiency analysis for multi-junction PV hetero-structures, in: Tanaka H., Yamashita, K., (Eds.), Photovoltaics: Developments, Applications and Impact. Nova Science, New York, pp. 213-247.
4. Neamen D.A., 2003. Semiconductor Physics and Devices, Mc. Graw Hill, Boston.
5. Shah, A., 2010. Thin-Film Silicon Solar Cells. EPFL Press, Lausanne.
6. Sze, S.M., 1981. Physics of Semiconductor Devices. John Wiley & Sons, New York.
7. Shah, A., R. Platz, H. Keppner, 1995. Thin Film Silicon Solar Cells: A Review and Selected Trends, Solar Energy Materials and Solar Cells 38, 501-520.
8. Froitzheim, A., R. Stangl, L. Elstner, M. Kriegel, W. Fuhs, "Afors-Het": A computer-program for the simulation of heterojunction solar cells to be distributed for public use, Hahn-Meitner-Institut Berlin, http://www.macs.hw.ac.uk/~michael/papers/hmi/aforshet.pdf
9. B. Van Zeghbroeck, 2007. Principles of Semiconductor Devices, http://ece-www.colorado.edu/~bart/book/
10. S. Vitanov, P. Vitanov, V. Palankovsky, 2008. 23rd European PV Solar Energy Conference Proceedings, 1743-1745
11. Golan G., Axelevitch A., Shavit R., "Photoelectric structure and method of manufactoring thereof", EP 2335290, H01L31/024, Published 22.06.2011